Catalysis Today 143 (2009) 218–224

Contents lists available at ScienceDirect

Catalysis Today

journal homepage: www.elsevier.com/locate/cattod

Reactivity and antimicrobial properties of nanostructured titanium dioxide

King Lun Yeung [a,*], Wai Kin Leung [b], Nan Yao [a], Shengli Cao [b]

[a] Department of Chemical Engineering, the Hong Kong University of Science and Technology, Clear Water Bay, Kowloon, Hong Kong, PR China
[b] Environmental Engineering Program, the Hong Kong University of Science and Technology, Clear Water Bay, Kowloon, Hong Kong, PR China

ARTICLE INFO

Article history:
Available online 20 November 2008

Keywords:
Titanium dioxide
Nanoparticles
Aerogel
Thin film
Photocatalyst
Photo-oxidation
Reactive oxygen species
Bactericidal

ABSTRACT

The photo-induced reactivity of three nanostructured titanium dioxides including TiO_2 nanoparticles (i.e., nano-TiO_2), titania–silica aerogel and nanotextured TiO_2 film, were investigated for gas phase photocatalytic oxidation of trichloroethylene and inactivation of *Bacillus subtilis* and *Escherichia coli* microbial cells. A correlation was observed between photoreactivity for TCE conversion and bactericidal activity within TiO_2 of similar nanostructures and composition (i.e., elemental and phase). This indicates that the photogenerated radical species from UV-irradiated TiO_2 responsible for TCE photo-oxidation also play a major role in the inactivation of microbial cells. The superb bactericidal activities of titania–silica aerogels (i.e., up to 6log reductions in viable *B. subtilis*) and nanotextured TiO_2 film (3.4log reduction) compared to commercial Degussa P25 TiO_2 (0.64log reduction) and optimum nano-TiO_2 (1.3log reduction) far exceeds the observed activity enhancement for TCE photo-oxidation. This implies that nanoscale chemical and structural environment also contribute towards the bactericidal activities.

1. Introduction

The remarkably high photoactivity of titanium dioxide (TiO_2) under near-UV irradiation proved to be effective for use in pollution abatement [1–3]. The recent works of Coronado and coworker's [4,5] demonstrated some practical aspects and challenges of TiO_2 application for air and water treatments, and developing efficient environmental photocatalysts remained an important goal. Indeed, a variety of TiO_2 materials synthesized in recent years including TiO_2 aerosols [6,7], aerogels [8–10], nanorods [11,12], nanotubes [13,14], nanocrystals [15–19] and mesoporous materials [20–23] show promising photoreactivity. Also, photo-induced superhydrophilicity and generation of reactive oxygen species (ROS) by photoactivated TiO_2 were linked to its antimicrobial properties [3]. Researches show that UV-irradiated TiO_2 could render nonviable microorganisms including bacteria and spores [24–27]. However, ROS generation had also been suggested for the cytoxicity of TiO_2 nanoparticles and their potential adverse impact on human health and environment [28,29]. Soria's research provides crucial understanding of the detailed mechanism of reactive specie generation in light activated TiO_2 and their relation to photoreactivity [17–19,30–33]. The same knowledge would be invaluable for elucidating the bactericidal activity of photoactive TiO_2 and toxicity of TiO_2 nanomaterials.

This work attempts to establish a link between photoreactivity of nanostructured TiO_2 for trichloroethylene (TCE) photo-oxidation in air with the observed antimicrobial properties against *Bacillus subtilis* and *Escherichia coli* cells with the underlying assumption that the reactive species generated by UVA activated TiO_2 responsible for the photocatalytic oxidation (PCO) of TCE also participated in the inactivation of microbial cells. This hypothesis was tested for three nanostructured TiO_2 materials including TiO_2 nanoparticles (i.e., nano-TiO_2), titania–silica aerogels and nanotextured TiO_2 films.

2. Experimental

2.1. Preparation of nanostructured TiO_2

Different synthesis methods were used to prepare TiO_2 nanoparticles (i.e., nano-TiO_2), titania–silica aerogels and nanotextured TiO_2 films investigated in this study.

TiO_2 nanoparticles were prepared by a modified sol–gel method described in previous works [34–36]. This approach has the advantage of producing anatase TiO_2 powder of uniform aggregate size and shape. Titanium isopropoxide (TIP, 98%, Aldrich) was reacted in an isopropanol–water solution at a constant temperature to yield spherical sols of 100 nm diameter. The sol was recovered, washed and dried to produce a free flowing powder. The anatase TiO_2 was crystallized from the amorphous powder by

* Corresponding author. Tel.: +852 2358 7123; fax: +852 2358 0054.
E-mail address: kekyeung@ust.hk (K.L. Yeung).

0920-5861/$ – see front matter © 2008 Elsevier B.V. All rights reserved.
doi:10.1016/j.cattod.2008.09.036

hydrothermal treatment at a neutral pH in a 150 mL, Teflon-line autoclave vessel (PTFE-4748, Parr Scientific). Anatase TiO_2 of different crystal sizes were obtained by simply varying the amounts of isopropanol in the alcohol–water solution used in the hydrothermal treatment. Comparisons were made with the commercial Degussa P25 TiO_2. Large rutile TiO_2 particles were prepared by microwave treatment at 650 W for 1 h of amorphous titania powder in 1 M HCl.

Titania–silica aerogels were prepared by a two-step, acid–base catalyzed method [37–39]. Tetramethyl orthosilicate (TMOS, 98%, Aldrich) in ethanol (99.9%, Merck) was prehydrolyzed with a dilute nitric acid solution (Fisher Scientific) at 323 K for 90 min under vigorous stirring to give a solution with a molar ratio of $1TMOS:2H_2O:0.005HNO_3:10.2C_2H_5OH$. A second solution was prepared by reacting an ethanol solution of TIP with acetylacetone (acac, 99+%, Sigma–Aldrich) in 1:1 mole ratio to give a solution containing xTIP:$x$acac:$2C_2H_5OH$. Measured amounts of the two solutions were mixed to obtain aerogels of Ti/Si ratios = 0.1, 0.5 and 1. A silica aerogel was prepared for comparison from an alcogel with a molar ratio of $1TMOS:4H_2O:0.065NH_3:12.25C_2H_5OH$. The reaction was completed with the addition of ammonia and resulting alcogel was aged for 10 days before ethanol supercritical drying. Ethanol supercritical drying crystallized anatase TiO_2 nanoparticles from the amorphous titania–silica aerogel. The prepared aerogel was calcined in Carbolite furnace at 723 K for 1 h to complete the TiO_2 crystallization.

Nanotextured TiO_2 films were prepared by spin-coating a titania sol on a nanotextured polymer surface produced by microwave-induced dewetting of ultrathin PMMA film (25,000 g mol^{-1}, Polysciences) on silicon wafer. The sol was prepared by reacting a solution of 4 mL titanium isopropoxide in 10 mL ethanol with an acidified ethanol solution containing 1 mL 2.3 M HNO_3 in 50 mL ethanol. The mixture was allowed to react at room temperature overnight. The resulting 0.20 mol L^{-1} titania sol was diluted with ethanol to 0.05 mol L^{-1} and spin-coated on the substrate at 6000 rpm. A plain TiO_2 film was also prepared by spin-coating the titania sol on the flat silicon substrate. The coated samples were calcined at 723 K for 2 h to remove the polymers and crystallize the anatase TiO_2.

2.2. Characterization of nanostructured TiO_2

The size of the nanostructured TiO_2 was determined by X-ray diffraction (XRD, Philips PW 1830) and transmission electron microscopy (TEM, JEOL JEM 2010F). The sample was ground into powder before analysis. X-ray diffraction was conducted at a scan rate of 0.05° using a Cu Kα X-ray source with a graphite monochromator. The weight fraction of the different TiO_2 phases was calculated from the integrated peak intensity and the crystal size was estimated from Scherrer equation. A direct observation of nanostructure TiO_2 is possible under TEM. The powder sample was dispersed in double deionized water and a drop of the suspension was placed onto the holey carbon-coated copper grid. Qualitative and quantitative elemental analyses of the thin sample were obtained by energy dispersive X-ray spectrometer. The TiO_2-coated plain and nanotextured samples were examined by atomic force microscope (Nanoscope IIIα, Digital Instruments).

Nitrogen physisorption of the powder samples was carried out in a Coulter SA 3100 to determine the specific surface area, pores size distribution and pore volume of the nanostructure TiO_2. The surface area of the crystallized anatase TiO_2 in the titania–silica aerogels was determined by 2-propanol dehydration reaction according to the procedure described by Hanprasopwattana et al. [40]. The catalyst samples were pretreated in helium at 373 K for an hour prior to the dehydration reaction at 533 K. Five reference anatase TiO_2 of known surface area (i.e., 15–90 $m^2\ g^{-1}$) were prepared for calibration. The nominal or bulk composition of the aerogel powder was determined by JEOL JSX-3201Z X-ray fluorescence spectroscopy (XRF). The XPS analysis was done in Physical Electronics PHI 5600 X-ray photoelectron spectroscopes with an Al monochromatic X-ray at a shallow angle to sample the topmost surface layer.

2.3. Photocatalytic oxidation activity of nanostructured TiO_2

The nanostructured TiO_2 were tested for photocatalytic oxidation of trichloroethylene. The powder TiO_2 photocatalysts were tested in a flat-plate photoreactor irradiated by five fluorescent black lamps (UVA, 365 nm, BLB Sankio Denki 6 W) placed 7 mm above the reactor window [34]. The photoreaction was carried out at ambient temperature and pressure, and 6 mg of TiO_2 coated on 6.3 cm^2 sample plate were used. The TCE (99.5%, Aldrich) was delivered to a constant temperature heat exchanger using a syringe pump (kdScientific 1000) and the vaporized TCE was mixed with 100 sccm dry synthetic air (22% O_2, Chun Wang Industrial gases HK Ltd.) to give a feed TCE concentration of 0.01 mM (i.e., 240 ppm). The outlet gases were separated using a GS-GASPRO capillary column (0.32 mm × 30 m) and analyzed using a gas chromatograph (HP 6890) equipped with thermal conductivity and flame ionization detectors. The reaction rate, turnover number (TON) and turnover frequency (TOF) were calculated from the steady-state TCE conversion. The TON and TOF of nano-TiO_2 were, respectively, calculated based on the total titanium content and TiO_2 surface area as determined by nitrogen physisorption. A complete mineralization of TCE was observed.

The silica and titania–silica aerogels were tested in an aerogel photoreactor described by Cao et al. [41]. The TCE was fed by a syringe pump and mixed with the dry synthetic air metered by an electronic mass flow controller (Sierra, Smart-Trak). A 40 sccm reactant mixture of 110 ppm TCE in dry air was used in the study and the aerogel was irradiated by a single fluorescent black lamp (Philips 6 W) at 710 μW/cm^2. The reaction was monitored by an on-line gas chromatograph (GC, HP 6890) equipped with thermal conductivity and flame ionization detectors. A 10% CarboWax 20 M on 80/100 Chromosorb W-HP column was used for the GC analysis. The TOF of titania–silica aerogels was calculated from the anatase TiO_2 surface area determined from 2-propanol dehydration reaction according to the method of Hanprasopwattana et al. [40] and accounting for the reactive volume calculated based on the UV penetration. No toxic intermediates and byproducts such as dichloroacetaldehyde, dichloroacetyl chloride and phosgene were detected in the reaction.

2.4. Antimicrobial properties of nanostructured TiO_2

The bactericidal properties of the nanostructured TiO_2 were tested for *B. subtilis* (15-5065A) and *E. coli* (15-5065A) purchased from Carolina Biological Supply. The bacteria stocks were kept on tryptone soya agar (TSA, Oxoid) plate (Difco) at 269 K. The bacteria cells were revitalized by sub-culturing a loopful of inoculum in 10 mL sterile Oxoid nutrient broth under gentle shaking for 18 h in a Gallenkamp incubator at 310 ± 0.1 K and 80 rpm. The viable cell count was determined by plate counting technique on TSA plate after serial dilution. The TiO_2 powder samples (0.2 g) were pressed into thin wafers and used unsupported for the bactericidal test, whereas the aerogel and nanotextured TiO_2 were supported on glass and silicon substrates, respectively. The aerogel samples were ground into a fine powder, dispersed in ethanol and deposited on a 10 mm glass disc to form a thin adherent film. The coated film was dried in an oven

at 333 K overnight. The pressed TiO_2 wafers, coated aerogel films, and both plain and nanotextured TiO_2 samples on silicon were sterilized in an autoclave (Hirayama, HA-300P) at 294 K for 20 min before use.

A hundred microliters of 10^7 cm^{-3} bacteria suspension was placed in contact with the sample and control (i.e., sterile glass) at ambient condition (296 ± 2 K, 70% R.H.) in a biosafety cabinet (NuAire, Nu-425-400E). The sample and control were exposed to UVA light (365 nm, 2650 $\mu W/cm^2$) for fixed irradiation times of 30 min. A 3 mL sterile nutrient broth (Nutrient broth no. 2, Oxoid) was added and after gentle shaking for 10 min, 100 μl aliquot was taken and cultured on TSA plate for 24 h at 310 ± 0.1 K to give the viable bacteria counts. The bactericidal tests were carried out in triplicate of five samples each. The cell membrane damage was investigated for the plain and nanotextured TiO_2 samples by measuring the malondialdehyde (MDA) produced by peroxidation of membrane lipid using the standard thiobarbituric acid assay [42].

3. Results and discussion

3.1. TiO_2 nanoparticles

Anatase TiO_2 nanoparticles were crystallized from the amorphous titania gel spheres following hydrothermal treatment in isopropanol–water solution. The nano-TiO_2 powder was free flowing and can be readily coated on surfaces or pressed into thin wafers (Fig. 1a). The shape and size of the starting gel spheres were retained during the crystallization [34] as shown by the transmission electron micrograph in Fig. 1b. The amorphous titania were consumed during the crystallization, transforming the gel sphere into a crystalline aggregate. Nano-TiO_2 powders of varying crystal sizes were obtained by using different isopropanol concentrations in the hydrothermal treatment. Fig. 3c shows the specific surface area of the Nano-TiO_2 decreases with increasing crystal size. The smallest nano-TiO_2 has an average crystal diameter of 3 nm and a specific surface area of 270 m^2 g^{-1}, whereas the largest prepared nano-TiO_2 measures 25 nm and 25 m^2 g^{-1}. The plots of turnover number and reaction rate for TCE photo-oxidation reaction in dry air are shown in Fig. 1d. The reaction shows a maximum rate for the 7 nm nano-TiO_2. A similar reaction trend was observed in an earlier study using dry oxygen for TCE photoreaction [17]. The electronic and structural effects (i.e., size and ensemble effects) are responsible for the observed optimum particle size for TCE photo-oxidation [34].

The bactericidal activity of the nano-TiO_2 was examined for *B. subtilis* vegetative cells under UVA irradiation of 4 J/cm^2, equivalent to 30 min exposure to UVA lamp (2650 $\mu W/cm^2$). The log reduction in viable *B. subtilis* after exposure to UVA shown in Fig. 1e follows a similar trend as the reactivity data plotted in Fig. 1d. The more photoactive nano-TiO_2 displays better bactericidal activity against *B. subtilis*. This is not surprising as the radical species generated during UV excitation of the TiO_2 photocatalyst are known to damage cell membrane by lipid peroxidation resulting in a change of membrane permeability and fluidity that make the cell less able to absorb nutrient and more vulnerable to osmotic stress [43,44]. Lu et al. [45] observed severe decomposition of cell wall and leakage of intracellular materials for cells exposed to UV-irradiated TiO_2. Aldehydes produced by the peroxidation reaction could further damage proteins and other cell components. ROS are also generated and react with biomolecules, inactivate enzymes and damage DNA by direct reaction with the nucleic acids [46,47,26,48].

A recent work by Hurum et al. [49] suggests that rutile TiO_2 enhances the photoactivity of mixed phase TiO_2 such as Degussa P25 by extending the photoactivity into visible wavelengths and generating catalytic hot spots at the interface regions between anatase and rutile particles. In a separate study, Tada and coworkers [50] suggests that higher charge separation efficiency caused by electron transfer across the anatase and rutile TiO_2 junction is mainly responsible for the enhanced photoactivity. Large anatase and rutile TiO_2 of comparable size to commercial Degussa P25 TiO_2 were prepared to investigate the effects of phase structure on the nano-TiO_2 photocatalytic and bactericidal activities. The transmission electron micrographs of the anatase and rutile TiO_2 are shown in Fig. 2a and b, respectively. The anatase TiO_2 has an average diameter of 18 nm, comparable to the width of the rutile TiO_2 crystals. The rutile TiO_2 particles are elongated and

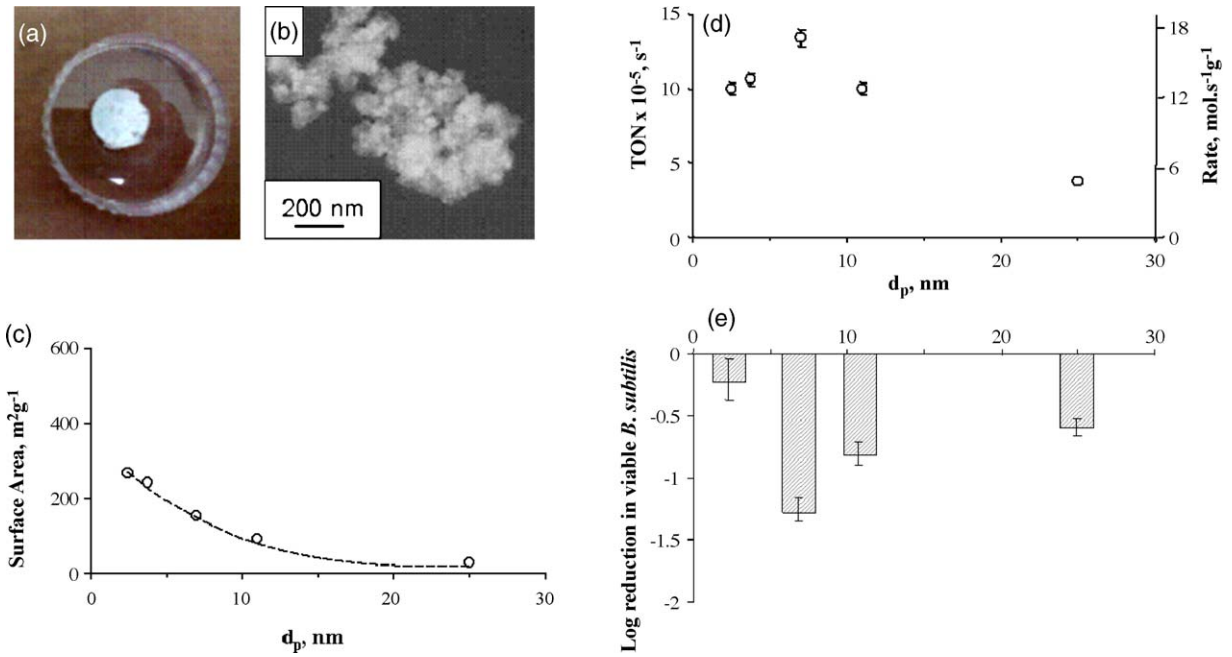

Fig. 1. Pictures of (a) pressed wafer of nano-TiO_2 powder and (b) high resolution TEM of nano-TiO_2 powder showing crystallized anatase TiO_2. Plots of (c) specific surface area, (d) turnover number for TCE photoreaction and (e) log reduction in viable bacteria (10^7 cm^{-3} *B. subtilis*, UVA irradiation 4 J cm^{-2}) for nano-TiO_2 of different particle sizes.

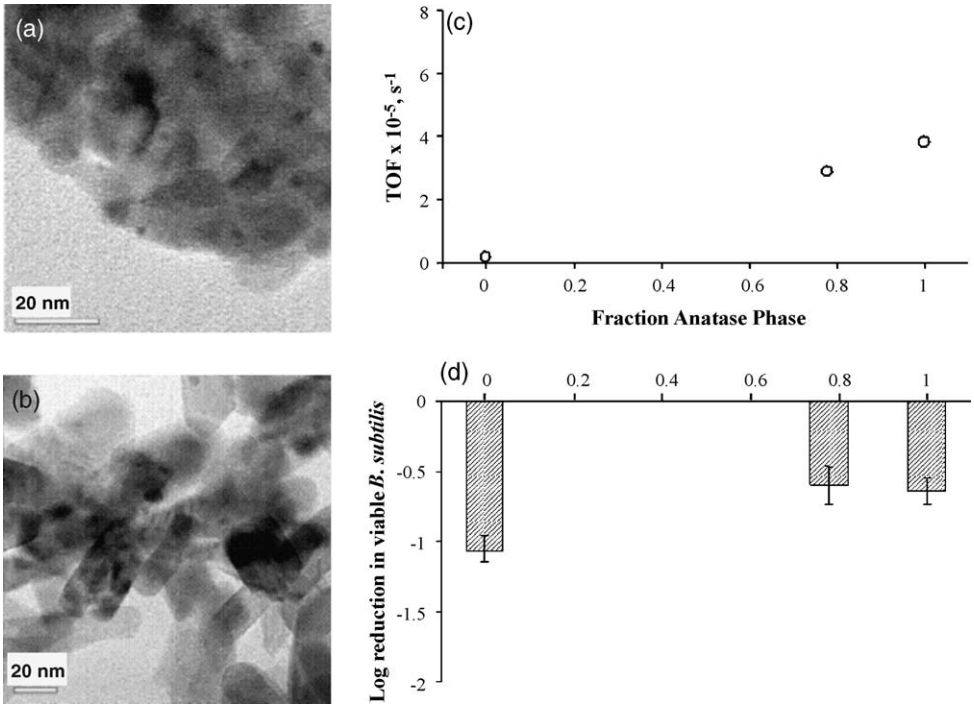

Fig. 2. Transmission electron micrographs of (a) anatase and (b) rutile nano-TiO_2. Plots of (c) turnover number for TCE photoreaction and (d) log reduction in viable bacteria (10^7 cm^{-3} *B. subtilis*, UVA irradiation 4 J cm^{-2}) for nano-TiO_2 of phase structures.

have an aspect ratio of 3.8. The anatase and rutile TiO_2, respectively, have BET surface areas of 48 ± 1 and 46 ± 2 m^2 g^{-1}, pore diameters of 5.4 and 7.1 nm, and pore volumes of 0.13 and 0.3 cm^3 g^{-1}. The P25 TiO_2 consisted of 18% rutile TiO_2 of 30 ± 5 nm and 82% anatase TiO_2 of 25 ± 3 nm, and displayed a surface area of 54 ± 2 m^2 g^{-1}, a pore diameter of 11.3 nm, and a pore volume of 0.16 cm^3 g^{-1}.

Fig. 2c plots of the turnover number for TCE photocatalytic oxidation over the anatase, rutile and mixed phase commercial TiO_2 photocatalysts. The rutile TiO_2 is essentially inactive due in part to the rapid rates of electron–hole recombination and only a trace of TCE conversion was observed during the photoreaction. The reaction rates are faster for the P25 TiO_2 and anatase TiO_2 in proportion to the anatase TiO_2 content of the catalyst. The mixed phase P25 TiO_2 has lower photoactivity compared to the pure phase anatase TiO_2 and activity enhancement is not apparent from the reaction data. The log reduction in viable *B. subtilis* vegetative cells after 30 min contact with UVA irradiated catalyst (i.e., 4 J/cm^2) is shown in Fig. 2d. It is surprising that the bactericidal activity of rutile TiO_2 (i.e., 1.1log reduction or 92% kill) is higher than the photoactive anatase and mixed phase TiO_2, which display 0.64 and 0.6log reduction in viable cells (i.e., 78 and 75% kill, respectively). Several researchers [51,52] reported that rutile TiO_2 is less bioreactive than the photoactive anatase TiO_2, but Gurr et al. [53] reported in their recent work that 200 nm rutile TiO_2 can induce hydrogen peroxide and oxidate DNA damages to cells. In this work, this could be partly attributed to the preparation of the rutile TiO_2 and its morphology. The rutile TiO_2 was prepared by microwave-assisted crystallization in acid solution and XPS detected surface Cl even after repeated washings. Besides ROS, there are other mechanisms for nanomaterial antimicrobial activity including physical disruption of cell membrane and interruption of energy transduction can occur when nanomaterials come into contact with the cell. Nanoparticle morphology and surface properties are believed to play a greater role in the latter mechanisms.

3.2. Titania–silica aerogels

The two-steps acid–base catalyzed method [39,54] allowed the preparation of crack-free, gas-permeable and photoactive titania–silica aerogels of high titanium content (i.e., up to Ti/Si = 1). A picture of titania–silica aerogel with nominal Ti/Si ratio of 1 is shown in Fig. 3a. X-ray diffraction indicated that 9 nm anatase TiO_2 were crystallized during the ethanol supercritical drying. The TiO_2 particle size displays a weak dependency on the titanium content of the aerogel (i.e., between Ti/Si = 0.1–1). The crystallized anatase TiO_2 nanoparticles were embedded within the titania–silica network (Fig. 3b) and were stable against sintering at high temperatures [38]. This allowed higher temperature treatment to obtain more crystalline anatase TiO_2 nanoparticles of large surface area, resulting in more photoactive catalysts [55]. Fig. 3c shows the BET surface area of the titania–silica aerogel decreases with the addition of the heavier titanium atom. The smaller surface area of the pure silica aerogel is due to the difference in its preparation. The anatase TiO_2 surface area in the mixed oxides aerogels was determined from the 2-propanol dehydration reaction [40] and plotted in Fig. 3c. The anatase TiO_2 surface area increases with the Ti loading of the aerogel.

The photocatalytic oxidation of TCE was performed in a homemade aerogel photoreactor at room temperature. By flowing the reactants through the porous aerogel, better mixing and faster mass transfer rate were obtained resulting in faster reaction rate. Fig. 3d plots the turnover frequency calculated based on the anatase TiO_2 surface area (cf. Fig. 3c), and takes into account that only the illuminated portion of the aerogel participates in the PCO reaction by calculating the reactive volume using the experimental UV penetration data [39]. The plot shows that the reaction rate increases in proportion to the Ti content of the mixed oxides aerogels. The TCE conversion over the silica aerogel is negligible and the aerogel could be considered inactive for the photoreaction. A similar observation was made for the amorphous titania–silica aerogels containing only Ti–O–Si sites [37]. However, partial

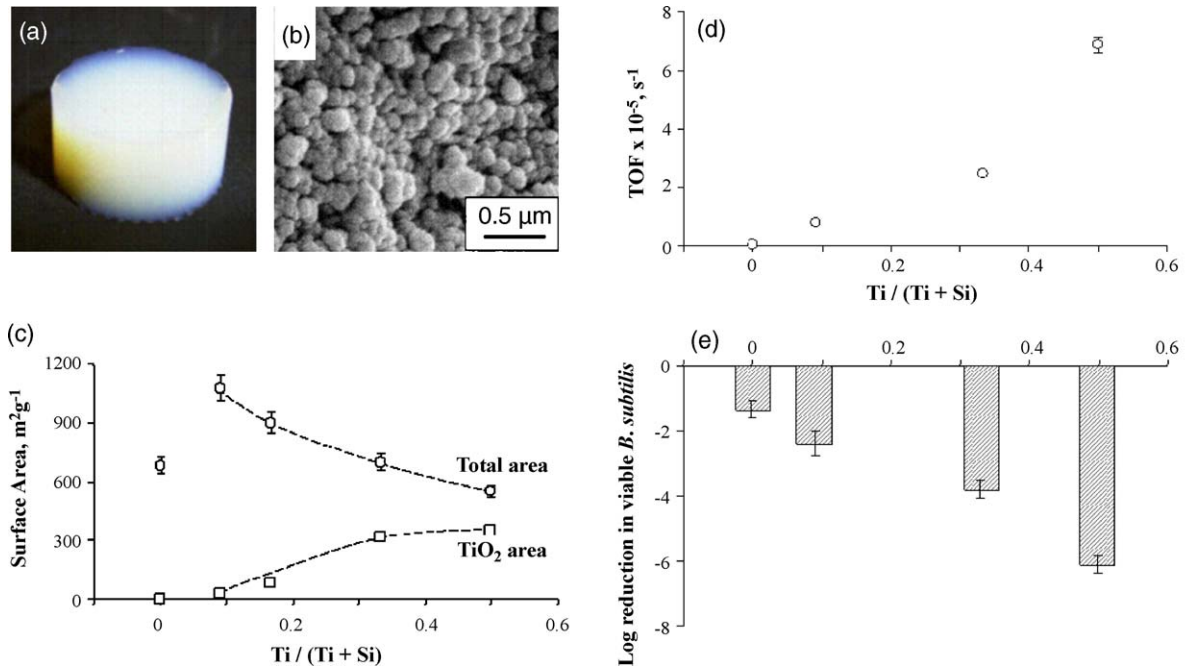

Fig. 3. Pictures of (a) freestanding titania–silica (Ti/Si = 1) aerogel and (b) scanning electron micrograph of the fractured aerogel. Plots of (c) BET surface area and anatase TiO_2 surface area, (d) turnover number for TCE photoreaction and (e) log reduction in viable bacteria (10^7 cm^{-3} *B. subtilis*, UVA irradiation 4 J cm^{-2}) for titania–silica aerogels of different titanium content.

oxidation products were detected in the silica and amorphous titania–silica aerogels during in situ DRIFTS study indicating limited reactivity [41]. Comparison between the titania–silica aerogel (Ti/Si = 1) and commercial Degussa P25 TiO_2 was made in the flat-plate photoreactor. The aerogel was ground into powder for the reaction experiment. The photoreaction was performed with 400 sccm dry air containing 110 ppm TCE. The aerogel catalyst displays an order of magnitude higher reaction rate of 4.3×10^{-5} mmol s^{-1} g^{-1} compared to P25 TiO_2 (i.e., 5.1×10^{-6} mmol s^{-1} g^{-1}). The enhanced photoactivity could be attributed to the more crystalline TiO_2 and larger catalytic surface of the titania–silica aerogels.

The bactericidal activity of the titania–silica aerogels was measured for *B. subtilis* cells and the results correlate well with the measured photoactivity of the catalyst as shown in Fig. 3e. It is clear from the figure that less number of bacteria remained viable on contact with the more photoactive aerogels. A 6log reduction or 99.9999% kill was obtained for the most active titania–silica aerogel (Ti/Si = 1). This value is five orders of magnitude better than the 1.3log reduction (i.e., 95% kill) from the best nano-TiO_2 photocatalyst (cf. Fig. 1e) or the 0.64log reduction (i.e., 77% kill) shown by P25 TiO_2. A glass plate serving as control sample gave 0.15log (29%) decrease in viable *B. subtilis* cells after 50 min UVA irradiation. It is speculated that the exceptionally high bactericidal activity of titania–silica aerogels originates from the greater number of radical species generated during UVA irradiation of the aerogels. The radicals are produced not only by the anatase TiO_2 crystals but also by the Ti–O–Si and Si–O–Si aerogel networks. Evidence for the latter could be seen from bactericidal activity of UVA irradiated silica aerogel and the observed reactivity of Ti–O–Si and Si–O–Si for partial oxidation reactions [41]. The enormous charged surface of the aerogel is also a contributing factor to its effectiveness against bacteria. Contact with the charged surfaces is known to interfere with the membrane function and interrupt energy transduction [56].

3.3. Nanotextured TiO_2 films

Although the ability to generate reactive oxygen species correlates well with the bactericidal activity of nanostructured TiO_2, it is clear from the experimental results there are other contributing factors that need to be considered including particle morphology and surface properties. In the titania–silica aerogel, the nanoscale chemical environment appeared important not only in stabilizing the anatase TiO_2 nanoparticles but also in radical production. The role of nanoscale environment was further investigated by preparing plain and nanotextured TiO_2 surfaces shown in Fig. 4a and b. The nanotextured film in Fig. 4b displays regular hemispherical bulges of 100 nm diameter over its entire surface. The films consisted of 9 nm anatase TiO_2 and were chemically identical. The nanoscale texturing alters the macroscale wetting property of the film transforming the superhydrophilic TiO_2 surface with wetting angle of 0° to a nonwetting surface (i.e., 90–120°). The observed lotus leaf effect of nanotextured TiO_2 is of great interest for self-cleaning surfaces.

Although nanotexturing increases the geometric area of the membrane by less than 2%, the bactericidal activity of the film increases by nearly two orders of magnitude compared to the plain TiO_2 film (Fig. 4c). The nanotextured TiO_2 is equally effective for the Gram positive *B. subtilis* (3.4log reduction, 99.96% kill) and Gram negative *E. coli* (2.6log reduction, 99.7% kill). The *B. subtilis* cells exposed to UVA irradiated nanotextured TiO_2 film displays elevated malondialdehyde level of 0.9 pmol/cell, which is significantly higher than the 0.5 pmol/cell observed from the plain TiO_2 film. This suggests that *B subtilis* suffered more extensive cell damage on the nanotextured TiO_2 film. It is believed that the nanoscale roughness increases contact points between the cell and the TiO_2 surface causing damages at multiple locations that eventually weaken and kill the microorganism. It is also speculated that like surface charges, the radical species could accumulate at the tip of the nano-protrusions creating reactive hot spots that could account for the orders of magnitude enhanced bactericidal activity.

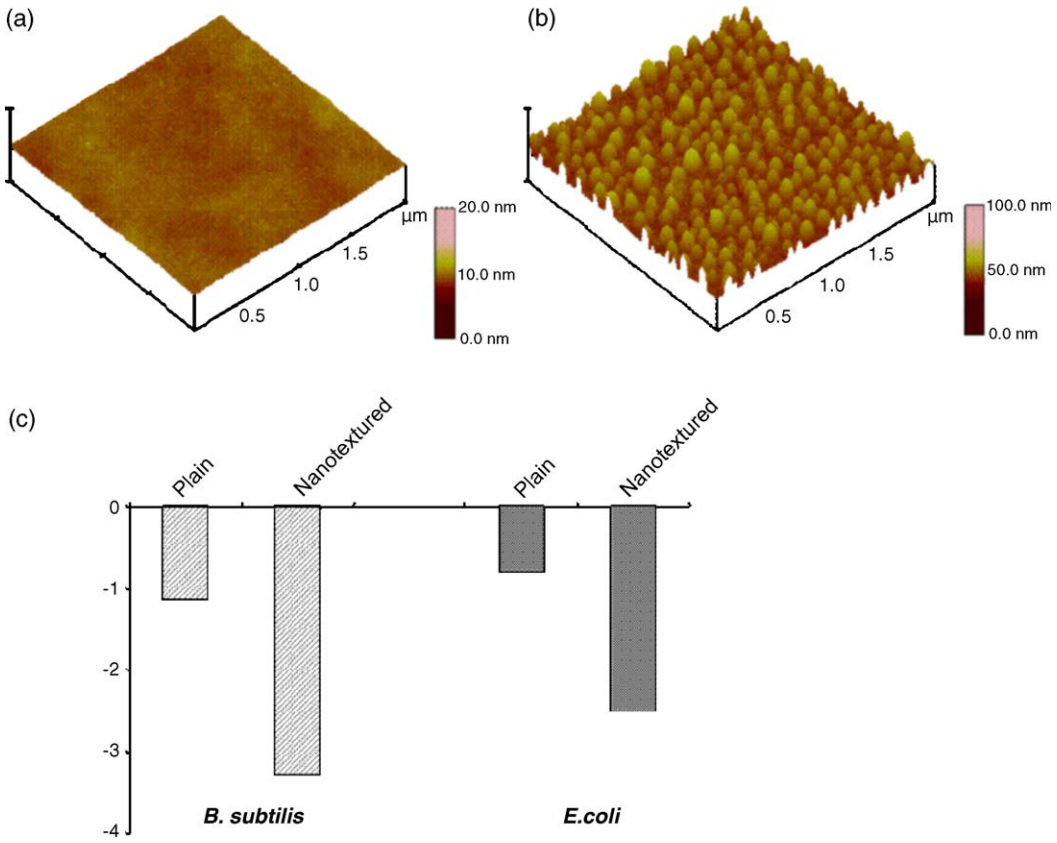

Fig. 4. Atomic force microscope images of (a) plain and (b) nanotextured TiO_2 films. (c) Plot of the log reduction in viable bacteria (UVA irradiation 4 J cm^{-2}) on plain and nanotextured TiO_2 films.

4. Concluding remarks

This work shows that the photoreactivity of nanostructured TiO_2 gives good indication of its antimicrobial activity. This suggests that the photo-generated reactive species responsible for photo-oxidation of TCE on TiO_2 participate either directly or indirectly in the inactivation of microorganisms. The elevated bactericidal activities of the poorly photoactive silica aerogel and inactive rutile TiO_2 suggest a heightened sensitivity of microorganisms even to weakly reactive photo-generated species. The material's nanostructure and surface properties could also cause physical disruption of cell membrane and interfere with membrane energy transduction resulting in microbial death. The superb bactericidal activities of titania-aerogels and nanotextured TiO_2 film clearly indicate that the nanoscale environment plays a potent role in the antimicrobial activity of these materials.

Acknowledgements

The authors would like to thank the financial support from the Hong Kong Innovation and Technology Commission and Chiaphua Industries Ltd. We also thank the technical help from the Material Preparation and Characterization Facility (MCPF) and the Advanced Engineering Material Facility (AEMF) of the Hong Kong University of Science and Technology.

References

[1] A. Mills, S. LeHunte, J. Photochem. Photobiol. A 108 (1997) 1.
[2] K. Hashimoto, H. Irie, A. Fujishima, Jpn. J. Appl. Phys. 44 (2005) 8269.
[3] O. Carp, C.L. Huisman, A. Reller, Prog. Sol. State Chem. 32 (2004) 33.
[4] J.M. Coronado, B. Sanchez, R. Portela, S. Suarez, J. Sol. Energy Eng.Trans. ASME 130 (2008) 011016.
[5] R. Portela, B. Sanchez, J.M. Coronado, R. Candal, S. Suarez, Catal. Today 129 (2007) 2223.
[6] C.R. Bickmore, K.F. Waldner, R. Baranwal, T. Hinklin, D.R. Treadwell, R.M. Laine, J. Eur. Ceram. Soc. 18 (1998) 287.
[7] C.B. Almquist, P. Biswas, J. Catal. 212 (2002) 145.
[8] L.K. Campbell, B.K. Na, E.I. Ko, Chem. Mater. 4 (1992) 1329.
[9] V. Strengl, S. Bakardjieva, J. Subrt, J. Szatmary, Micropor. Mesopor. Mater. 91 (2006) 1.
[10] S. Yoda, D.J. Suh, T. Sato, J. Sol–Gel Sci. Technol. 22 (2001) 75.
[11] J. Joo, S.G. Kwon, T. Yu, M. Cho, J. Lee, J. Yoon, T. Hyeon, J. Phys. Chem. B 109 (2005) 15297.
[12] X. Peng, A. Chen, J. Mater. Chem. 14 (2004) 2542.
[13] P. Hoyer, Langmuir 12 (1996) 1411.
[14] C. Aprile, A. Corma, H. Garcia, Phys. Chem. Chem. Phys. 10 (2008) 769.
[15] M. Qamar, C.R. Yoon, H.J. Oh, N.H. Lee, K. Park, D.H. Kim, K.S. Lee, W.J. Lee, S.J. Kim, Catal. Today 131 (2008) 3.
[16] M. Wu, G. Li, D. Chen, G. Wang, D. He, S. Feng, R. Xu, Chem. Mater. 14 (2002) 1974.
[17] A.J. Maira, K.L. Yeung, J. Soria, J.M. Coronado, C. Belver, C.Y. Lee, V. Augugliaro, Appl. Catal. B 29 (2000) 327.
[18] A.J. Maira, J.M. Coronado, V. Augugliaro, K.L. Yeung, J.C. Conesa, J. Soria, J. Catal. 202 (2001) 413.
[19] J.M. Coronado, A.J. Maira, J.C. Conesa, K.L. Yeung, V. Augugliaro, J. Soria, Langmuir 17 (2001) 5368.
[20] D.M. Antonelli, J.Y. Ying, Angew. Chem. Int. 34 (1995) 2014.
[21] F. Bosc, A. Ayral, P.A. Albouy, L. Datas, C. Guizard, Chem. Mater. 16 (2004) 2208.
[22] J.G. Yu, J.C. Yu, W.L.K. Ho, Z.T. Jiang, New J. Chem. 26 (2002) 607.
[23] Y. Yamauchi, F. Takeuchu, S. Todoroki, Y. Sakka, S. Inoue, Chem. Lett. 37 (2008) 72.
[24] A. Vohra, D.Y. Goswami, D.A. Deshpande, S.S. Block, Appl. Catal. B: Environ. 64 (2006) 57.
[25] C.Y. Lin, C.S. Li, Aerosol Sci. Technol. 37 (2003) 939.
[26] Y. Kikuchi, K. Sunada, T. Iyoda, K. Hashimoto, A. Fujishima, J. Photochem. Photobiol. A 106 (1997) 51.
[27] K. Sunada, T. Watanabe, K. Hashimoto, J. Photochem. Photobiol. A 156 (2003) 227.
[28] C.A.J. Dick, D.M. Brown, K. Donaldson, V. Stone, Inhal. Toxicol. 15 (2003) 39.
[29] T.C. Long, N. Saleh, R.D. Tilton, G.V. Lowry, B. Veronesi, Environ. Sci. Technol. 40 (2006) 4346.
[30] J.M. Coronado, S. Kataoka, I. Tejedor-Tejedor, M.A. Anderson, J. Catal. 219 (2003) 219.

[31] J. Soria, J. Sanz, I. Sobrados, J.M. Coronado, F. Fresno, M.D. Hernández-Alonso, Catal. Today 129 (2007) 240.
[32] J. Soria, J. Sanz, I. Sobrados, J.M. Coronado, A.J. Maira, M.D. Hernández-Alonso, F. Fresno, J. Phys. Chem. C 111 (2007) 10590.
[33] J.M. Coronado, J. Soria, Catal. Today 123 (2007) 37.
[34] A.J. Maira, K.L. Yeung, C.Y. Lee, P.L. Yue, C.K. Chan, J. Catal. 192 (2000) 185.
[35] K.L. Yeung, A.J. Maira, J. Stolz, E.W.C. Hung, N.K.C. Ho, A.-C. Wei, J. Soria, K.-J. Chao, P.-L. Yue, J. Phys. Chem. B 106 (2002) 4608.
[36] K.L. Yeung, S.T. Yau, A.J. Maira, J.M. Coronado, J. Soria, P.L. Yue, J. Catal. 219 (2003) 107.
[37] S. Cao, K.L. Yeung, P.L. Yue, Appl. Catal. B: Environ. 68 (2006) 99.
[38] S. Cao, N. Yao, K.L. Yeung, J. Sol–Gel Sci. Technol. (2008) 1.
[39] S.L. Cao, K.L. Yeung, J.K.C. Kwan, P.M.T. To, S.C.T. Yu, Appl. Catal. B, in press.
[40] A. Hanprasopwattana, S. Srinivasan, A.G. Sault, A.K. Datye, Langmuir 12 (1996) 3173.
[41] S. Cao, K.L. Yeung, P.L. Yue, Appl. Catal. B: Environ. 76 (2007) 64.
[42] H. Esterbauer, K.H. Cheeseman, Methods Enzymol. 186 (1990) 407.
[43] P.C. Maness, S. Smolinski, D.M. Blake, Z. Huang, E.J. Wolfrum, W.A. Jacoby, Appl. Environ. Microbiol. 65 (1999) 4094.
[44] E. Cabiscol, J. Tamarit, J. Ros, Int. Microbiol. 3 (2000) 3–10.
[45] Z.X. Lu, L. Zhou, Z.L. Zhang, W.L. Shi, Z.X. Xie, D.W. Pang, P. Shen, Langmuir 19 (2003) 8765.
[46] T. Hancock-Chen, J.C. Scaiano, J. Photochem. Photobiol. B 57 (2000) 193.
[47] H. Hidaka, J. Photochem. Photobiol. A 108 (1997) 197.
[48] J.A. Imlay, Ann. Rev. Microbiol. 57 (2003) 395.
[49] D.C. Hurum, A.G. Agrios, K.A. Gray, T. Rajh, M.C. Thurnauer, J. Phys. Chem. B 107 (2003) 4545.
[50] T. Kawahara, Y. Konishi, H. Tada, N. Tohge, J. Nishii, S. Ito, Angew. Chem. Int. Ed. 41 (2002) 2811.
[51] D.G. Olmedo, D.R. Tastat, P. Evelson, M.B. Guglielmotti, R.L. Cabrini, J. Biomed. Mater. Res. A 84 (2008) 1087.
[52] C.M. Sayes, R. Wahi, P.A. Kurian, Y.P. Liu, J.L. West, K.D. Ausman, D.B. Warheit, V.L. Colvin, Toxicol. Sci. 92 (2006) 174.
[53] J.R. Gurr, A.S.S. Wang, C.H. Chen, K.Y. Jan, Toxicology 213 (2005) 66.
[54] N. Yao, S.L. Cao, K.L. Yeung, Micropor. Mesopor. Mater., in press.
[55] K.Y. Jung, S.B. Park, Appl. Catal. B: Environ. 25 (2000) 249.
[56] T. Mashino, K. Okuda, T. Hirota, M. Hirobe, T. Nagano, M. Mochizuki, Bioorg. Med. Chem. Lett. 9 (1999) 2959–2962.